CrossMark

Microtubule guiding in a multi-walled carbon nanotube circuit

Aurélien Sikora[1] · Javier Ramón-Azcón[2,3] · Mustafa Sen[4,5] · Kyongwan Kim[1] ·
Hikaru Nakazawa[6] · Mitsuo Umetsu[6] · Izumi Kumagai[6] · Hitoshi Shiku[1,4] ·
Tomokazu Matsue[1,4] · Winfried Teizer[1,7,8]

Abstract In nanotechnological devices, mass transport can
be initiated by pressure driven flow, diffusion or by employing
molecular motors. As the scale decreases, molecular motors
can be helpful as they are not limited by increased viscous
resistance. Moreover, molecular motors can move against dif-
fusion gradients and are naturally fitted for nanoscale trans-
portation. Among motor proteins, kinesin has particular po-
tential for lab-on-a-chip applications. It can be used for
sorting, concentrating or as a mechanical sensor. When bound
to a surface, kinesin motors propel microtubules in random
directions, depending on their landing orientation. In order to
circumvent this complication, the microtubule motion should
be confined or guided. To this end, dielectrophoretically
aligned multi-walled-carbon nanotubes (MWCNT) can be
employed as nanotracks. In order to control more precisely
the spatial repartition of the MWCNTs, a screening method
has been implemented and tested. Polygonal patterns have
been fabricated with the aim of studying the guiding and the
microtubule displacement between MWCNT segments.
Microtubules are observed to transfer between MWCNT seg-
ments, a prerequisite for the guiding of microtubules in
MWCNT circuit-based biodevices. The effect of the
MWCNT organization (crenellated or hexagonal) on the MT
travel distance has been investigated as well.

Keywords Carbon · Nanotube · Microtubule · Kinesin ·
Dielectrophoresis

1 Introduction

In cells, sophisticated motor proteins provide the force necessary
for intracellular transport and chromosome migration. For exam-
ple, the mechano-enzyme kinesin-1 (hereafter referred to as
kinesin) converts chemical energy into mechanical work with a
yield as high as 60 % (Hess et al. 2004; Hwang and Lang 2009).
Consuming one Adenosine Triphosphate (ATP) molecule per
16 nm step which results in a 8 nm displacement, kinesin is able
to perform about 100 step/s, at a speed of 800 nm/s (Howard
et al. 1989). Moreover, by producing a force reaching 7 pN

✉ Winfried Teizer
teizer@tamu.edu

1 WPI Advanced Institute for Materials Research, Tohoku University,
2-1-1 Katahira, Sendai 980-8577, Japan

2 Department of Chemical and Biomolecular Nanotechnology,
Advanced Chemical Research Institute of Catalonia (IQAC-CSIC),
Jordi Girona 18-26, Barcelona 08034, Spain

3 Nanobiotechnology for Diagnostics (Nb4D) Group, IQAC-CSIC,
Jordi Girona 18-26, 08034 Barcelona, Spain

4 Graduate School of Environmental Studies, Tohoku University,
Sendai 980-8579, Japan

5 Department of Biomedical Engineering, Faculty of Engineering and
Architecture, Izmir 35620, Turkey

6 Department of Biomolecular Engineering, Graduate School of
Engineering, Tohoku University, Sendai 980-8579, Japan

7 Materials Science and Engineering, Texas A&M University, College
Station, TX 77843-3003, USA

8 Department of Physics and Astronomy, Texas A&M University,
College Station, TX 77843-4242, USA

(Svoboda and Block 1994), kinesin can transport micrometer size cargo (Böhm et al. 2001). The steps are performed along a biopolymer track, the microtubule (MT). Kinesin is characterized by its high processivity, i.e. its ability to stay attached to the MT after each step. Experimentally, this property results in a detachment from the track after a travel distance of a few micrometers (Romberg et al. 1998) and can be observed by labeling the motors, for example with quantum dots (Sikora et al. 2012). In a reversed configuration, when attached to a surface, kinesin can propel the MT. As several motors can interact with the MT, which can measure a few tens of micrometers long, the detachment occurs only after traveling at least the same distance, depending on the MT length and the kinesin density (Howard et al. 1989). In addition, due to its intrinsic size, the carriage capacity of a MT is more advantageous than kinesin. Thus, this configuration is more attractive for transport applications. The main issue arises from the random direction of the MT gliding. This has been solved by implementing a confinement strategy. For example, it is possible to direct MTs and prevent their escape by trapping them in enclosed channels (Huang et al. 2007). However, the downscaling of such devices is limited by the lithography resolution. It is also possible to directly pattern the MT using electrodes (Noel et al. 2009) or to guide them with micro wires (Kim et al. 2014a, b, 2015). In this case, due to the high flexural rigidity of the MT (Hawkins et al. 2010), its preferential orientation depends on the curvature of the wire. The higher the curvature, the more parallel to the wire they glide. If the MT binds perpendicular to the wire axis, it binds to a smaller number of kinesin proteins, making this configuration less stable. Here, we investigate the extreme case of multi-walled carbon nanotubes (MWCNTs). Their intrinsic size and their chemical inertia make them a good candidate for elaborating nanotracks in a protein friendly environment. However, to achieve this, MWCNTs have to be organized using one of several alignments techniques. For example, MWCNTs can be aligned by molecular combing (Gerdes et al. 1999) or by direct manipulation with an atomic force microscope (AFM) tip (Postma et al. 2000). Molecular combing requires drying and therefore is not compatible with functional proteins. An AFM tip manipulates carbon nanotubes one by one and, therefore, is slow and inconvenient for large scale alignment. MWCNTs can also be organized by dielectrophoresis (DEP) (Chen et al. 2001). When exposed to an AC electric field, metallic MWCNTs get polarized and orient themselves parallel to the field lines. This technique is easy to apply and can be performed in water, making it compatible with protein functionalized MWCNTs. Recently, we have shown that it is possible to align and attach MWCNTs on a functionalized surface in order to build tracks allowing MT gliding (Sikora et al. 2014). Here we show how the width of the MWCNT track can be modulated and how to limit the MWCNT dispersion. Moreover, MT transfers between MWCNT segments have still to be explicitly observed and analyzed for the further development of MWCNT based biodevices. Thus, we present here a

new configuration of electrodes allowing the investigation of MT gliding on a hexagon and octagon shaped MWCNT track. Using these geometries, the displacement of MT between MWCNT segments can be studied with two different angles and therefore, the role of the curvature in the guiding performance can be investigated. Furthermore, this arrangement potentially allows monitoring the gliding of a MT along an unlimited path without exiting the field of view.

2 Materials and methods

2.1 Hexagonal and octagonal device fabrication

The chip device for the hexagonal MWCNTs alignment was fabricated using contact lithography. The chip contains two layers. First, in order to fabricate the six electrodes facing each other in a hexagonal manner (Fig. 1b), a Ti/Pt layer was sputtered on an ultrasound and oxygen plasma treated glass slide. Second, a thin SU-8 layer was deposited in order to insulate all the electrodes and form a circle shaped channel around the tips of the electrode, which accommodates the hexagonal CNT alignment. The width and depth of the channel are 12 and 5 μm, respectively. The distance between the electrodes is approximately 15 μm. The octagonal device fabrication followed the same protocol, using 8 electrodes instead of 6.

In order to modify the channel bottom surface with a self-assembled monolayer (SAM) necessary for MWCNT attachment, the chip was first treated with an oxygen plasma for 1 min to both clean it and create hydroxyl groups on the surface. The biotinylation treatment and the MWCNT functionalization followed the protocol described elsewhere (Sikora et al. 2014). After surface modification, a 50 μm thick spacer was placed between the chip and a glass substrate to form a chamber for introduction of 0.4 mg/ml streptavidin modified MWCNTs. Prior to the introduction of the functionalized MWCNTs, the solution was treated with ultrasound in order to minimize aggregations, which ensured the integrity of the DEP alignment. The final streptavidin modified MWCNT solution for DEP alignment was introduced with 5 % PBS. Once the flow of MWCNTs in the chamber stopped, a sinusoidal AC excitation (1 MHz, peak voltage: 4 V) was applied between the electrodes for approximately 5 min using a multifunction generator (WF1948, NF Co., Japan) as shown in Fig. 1a. Subsequently, mobile MWCNTs were removed by replacing the fluid in the chamber with Milli-Q water containing 5 % PBS twice. Using this strategy, streptavidin modified MWCNTs were successfully aligned in a hexagonal (Figs. 1c and 2a) or octagonal manner (Fig. 2b). The MWCNT alignment was observed and recorded using an optical microscope (DMIRE2; Leica Co., Germany) equipped with a digital CCD camera (DFC350X; Leica Co., Germany).

Fig. 1 **a** Schematic describing the hexagonal alignment method. *Red* and *blue* electrodes are exposed to inverted potentials. **b** Hexagonal device before introduction of the MWCNTs. **c** Hexagonal device after MWCNTs alignment and washing
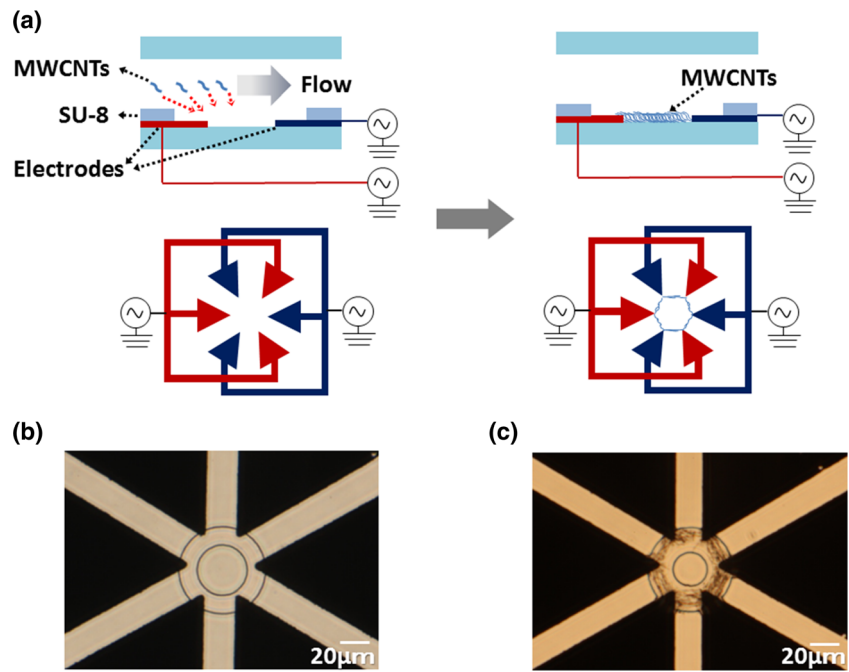
2.2 Crenellated device

The fabrication method has been described elsewhere (Sikora et al. 2014). Streptavidinated MWNCTs were aligned by DEP between indium tin oxide electrodes (see Fig. 3a). An additional SU-8 layer has been deposited in order to confine the spreading of the MWCNTs, which were attached on a biotinylated glass surface.

2.3 Microtubules and kinesin construct

A 3:7 mixture of rhodamine-labeled/non labeled tubulin was polymerized from commercially available porcine tubulin (Cytoskeleton, USA) according to a protocol described elsewhere (Maloney et al. 2011). The kinesin used in the octagonal device consists in the 400 first amino acids of *Neurospora Crassa's* kinesin-1 (NCkin) fused with a biotin carboxyl

Fig. 2 **a** Bright field image of MWCNTs aligned between electrodes in a hexagonal configuration. **b** Fluorescence and bright field microscopy image of the MWCNTs aligned in an octagonal configuration (image size: 51.2×51.2 μm). **c** Fluorescence microscopy images of a MT, indicated by a *blue arrow*, gliding along MWCNTs (image width: 19.8 μm). The path of the MT is shown by a *green dotted line*. The images were extracted from the movie available in the supporting information
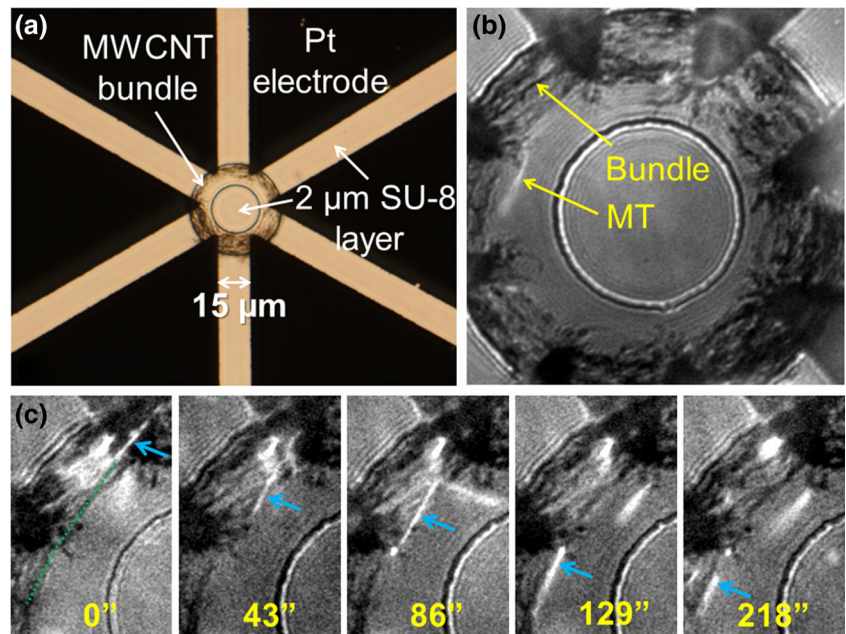
Fig. 3 **a** Bright field images of the aligned MWCNTs in the case of low and high concentration of MWCNTs. The space between two electrodes indicated by an arrow is 100 μm. The *yellow dashed line* indicates the location of the intensity profiles. Insets show in detail the organization of the MWCNTs. **b** Intensity profiles mentioned in Fig. 3a in the case of low (*left*) and high (*right*) MWCNT concentration
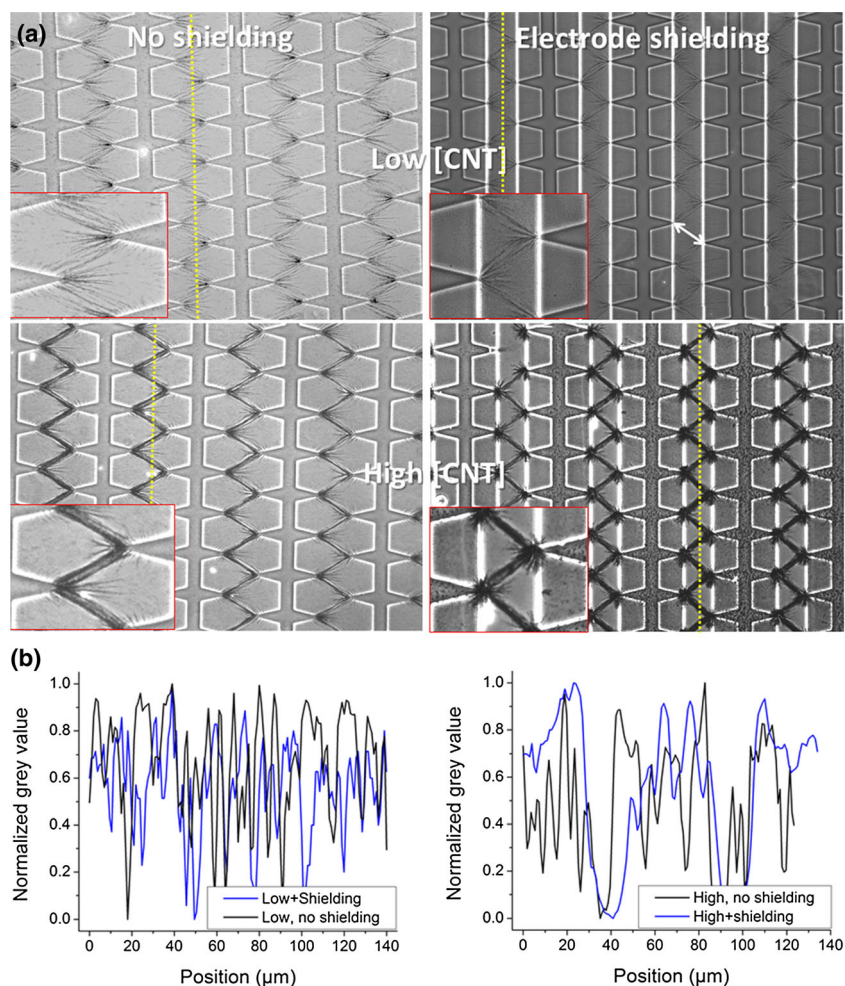
carrier protein (BCCP) (Kim et al. 2011), a short linker (Cloutier et al. 2000) and a hexahistidine tag. NCkin's DNA was purchased from Life Technologies. In order to insert the NCkin's gene, the pRA2 expression vector was digested with NcoI and SacII enzymes. The NCkin's gene was ligated using a DNA Ligation Kit Mightly mix (TaKaRa Co., Ltd). The gene sequence was checked with a 3130xl Genetic Analyzer (Applied Biosystems). The protein was then expressed in E. coli following a standard protocol (Oliveira et al. 2012). In the case of the crenellated device, a truncated biotinylated kinesin-1 from *Drosophilia Melanogaster* (DmKin) has been used. Details on the construct and its expression are available elsewhere (Kim et al. 2014a).

2.4 Motility assays

After the alignment of the MWCNTs, the flow cell was successively flushed with BRB80 buffer (Olmsted and Borisy 1975), BRB80 complemented with 0.5 mg mL^{-1} casein and incubated 5 min at room temperature. Diluted kinesin in BRB80 buffer (final concentrations: 0.8 μM for NCkin, 4 μM for DmKin) complemented with ATP (1 mM) was introduced in the chamber

and incubated for 5 min. MT, diluted in BRB80 buffer (2.5 mg mL^{-1}) complemented with oxygen scavenger (20 μg mL^{-1} glucose oxidase, 8 μg mL^{-1} catalase, 20 mM glucose), β-mercaptoethanol (0.5 %v/v), 2 mM ATP and 10 μM taxol, were introduced in the chamber and the glass slide was immediately mounted on an IX-71 (Olympus, Japan) microscope. The same protocol was employed in the case of graphite. HOPG (SPI-3 Grade, Alliance Biosystems, Japan) was cleaved using double-sided tape. The resulting graphite film was then stuck on a glass slide and assembled in a flow cell.

2.5 Image acquisition and analysis

Fluorescence microscopy videos and images have been acquired using a digital CCD camera (Hamamatsu, Image EM) with the software Metamorph. Data were processed with ImageJ. The "roughness" R_a has been calculated based on intensity profiles of the images, following the standard formula $1/n \sum_{i=1}^{n} I_i$, with I being the value of the black background. For purposes of comparison between images, intensity values have been normalized. Width measurements were performed by fitting peaks of the image profiles with a Gaussian. Bundle density was estimated

Table 1 Characteristics of the MWCNT organization

Condition	MWCNT concentration (mg mL^{-1})	$R_a \pm SD$ (a.u.)	Bundle density (μm^{-1})	Maximum width (μm)
Shielding	0.2	0.30±0.13	0.23	3.7
Shielding	2	0.56±0.27	0.1	30
No shielding	0.5	0.15±0.09	0.21	3.5
No shielding	1	0.47±0.16	0.21	55

by counting the number of peaks of the profiles. MT tracking was performed using the MTrackJ plugin for ImageJ.

3 Results

First, the arrangement of the MWCNTs after DEP alignment has been studied in a crenellated electrode configuration (Sikora et al. 2014). In order to avoid the spreading of MWCNTs between the electrodes, we have implemented an additional layer of resist acting as a screen for the electric field. This system allows the confinement of MWCNTs between the electrodes, limiting potential displacement of MTs in unintended directions (see Fig. 3a). The effects of the MWCNT's concentration and the additional SU-8 layer (shielding) is shown in Fig. 3a. The magnified images show that MWCNT bundles are barely present on the sides of the shielded electrodes, proving the screening efficiency of the SU-8 layer. To characterize the surface state, the "roughness" R_a has been estimated based on intensity profiles (Fig. 3b) performed on the bright field microscopy images (Fig. 3a). The results have been assembled in Table 1. According to these measurements, the maximum width and the "roughness" of the MWCNT bundles increase with the MWCNT concentration. The bundle density does not seem strongly affected by the concentration change or the presence of the SU-8 layer. This can be logically explained by the insertion of a larger amount of MWCNTs. They aggregate, thus widening the bundles, instead of forming additional tracks.
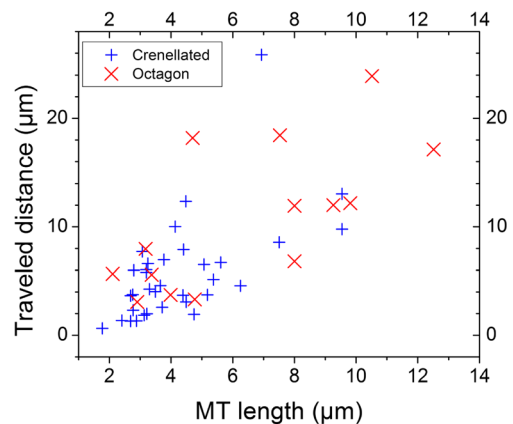
We employed the same screening strategy to investigate the feasibility of MWCNT alignment in an octagonal and hexagonal shape configuration. Figure 2a and b show the organized MWCNTs. The circular resist layer prevents the formation of

bridges between opposite electrodes. The outer resist layer confines the nanotubes near the electrodes and protects the organized structure during fluid exchange. After washing, no MWCNTs could be seen outside the hexagon and the octagon area. The MWCNT structure was still preserved after several flushes.

In order to study the gliding of MT on MWCNT tracks, motility assays were performed (Howard et al. 1989). Figure 2c shows fluorescence microscopy images of the MT motion along the MWCNT track. Using an octagonal configuration, the passage between two MWCNT segments could be observed (see Movie1). MTs can pass the platinum electrode and transit towards the next segment. It demonstrates the feasibility of a full MWCNT circuit designed for MT shuttle transportation. Characteristics of the gliding are assembled in the Table 2. In the case of the octagonal device, the probability P of travelling a distance longer than the MT's length was about 0.79. According to Howard's model (Howard et al. 1989), this translates to a kinesin density of about 160 μm^{-2}. Assuming that all the introduced kinesin molecules are adsorbed, our calculated kinesin density estimation is eighty times higher. In this case, as the probability of non-detachment reaches one, each MT should glide longer than its own length. This difference may be explained by the surface topology. Indeed, the potential contact area between a MT and the surface is smaller in the case of a MWCNT than on a flat surface, reducing their range of interaction. Gliding assays performed on graphite with a similar kinesin density confirm this and show that every MT travels more than their own length before detachment.

Table 2 MT gliding characteristics for the octagonal, the crenellated device and on graphite: average traveled distance before detachment, average MT length used in the assay and the measured probability P of traveling a distance longer than the MT's length. The uncertainty given is the standard deviation

	Traveled distance (μm)	MT length (μm)	P
Octagonal device	10±6.6	6.5±2.8	0.79
Crenellated device	5.8±4.7	4.3±1.9	0.59
Graphite	No observed detachment	10±6.8	1

Fig. 4 MT travel distance as a function of the MT length measured in the crenellated and in the octagonal device

The average travelled distance is shorter in the case of the crenellated device. This may be explained by the smaller average length of the MT inserted in the flow cell. The longer the MT the more probable its non-detachment, as the number of potential kinesin binding sites increases. This trend can be observed on the Fig. 4.

The guiding efficiency has been estimated by measuring the angle difference between the MT path and the MWCNT track formed between two adjacent electrodes. The average angular deviation is 28 ± 23 ° (standard deviation, $N=20$). The guiding may be caused by the channel confinement (Moorjani et al. 2003). In order to assess this effect, the same experiment has been performed without MWCNTs. We found a larger average angular deviation ($34\pm26°$, $N=41$). In the case of a random displacement, the deviation should be near 45°. Thus, despite the large width of the circular channel, there appears to be a preferential orientation due to the curvature of the resist layer. The guiding may be improved by narrowing the MWCNT track width, reducing the orientation possibilities of the bound MT. Despite them not being visible microscopically, Scanning Electron Microscopy investigations revealed that single MWCNT tracks are present as well (Sikora et al. 2014), demonstrating the feasibility of very narrow tracks.

4 Conclusions

Functionalized MWCNTs can be rapidly aligned by DEP forming visible bundles of micrometer size width. The measurements show that the bundle width increases with the MWCNT concentration. The spreading of MWCNTs can be limited by employing an additional resist layer acting as an electric field screen. The MT guiding ability of MWCNT tracks has been studied. MTs are able to transit between MWCNT segments and they follow the MWCNT orientation with an average angular deviation of about 27°. This work demonstrates the potential of MWCNTs for the elaboration of molecular motor powered biodevices and opens the way to MWCNT track development. MWCNTs present additional interesting properties that can be useful in nanotechnological devices. For example, their metallic character enables them to work as electrodes and can be exploited in order to control MT remotely or to function as sensors.

References

K.J. Böhm, R. Stracke, P. Mühlig, E. Unger, Nanotechnology **12**, 238 (2001)

X.Q. Chen, T. Saito, H. Yamada, K. Matsushige, Appl. Phys. Lett. **78**, 3714 (2001)

S.M. Cloutier, S. Couty, A. Terskikh, L. Marguerat, V. Crivelli, M. Pugnières, J.C. Mani, H.J. Leisinger, J.P. Mach, D. Deperthes, Mol. Immunol. **37**, 1067–1077 (2000)

S. Gerdes, T. Ondarçuhu, S. Cholet, C. Joachim, Europhys. Lett. **48**, 292 (1999)

T. Hawkins, M. Mirigian, M. Selcuk Yasar, J.L. Ross, J. Biomech. **43**, 23–30 (2010)

H. Hess, G.D. Bachand, V. Vogel, Chem. Eur. J. **10**, 2110–2116 (2004)

J. Howard, A.J. Hudspeth, R.D. Vale, Nature **342**, 154–158 (1989)

Y.M. Huang, M. Uppalapati, W.O. Hancock, T.N. Jackson, Biomed. Microdevices **9**, 175–184 (2007)

W. Hwang, M.J. Lang, Cell Biochem. Biophys. **54**, 11–22 (2009)

D.-M. Kim, M. Umetsu, K. Takai, T. Matsuyama, N. Ishida, H. Takahashi, R. Asano, I. Kumagai, Small **7**, 656–664 (2011)

K. Kim, A. Liao, A. Sikora, D. Oliveira, H. Nakazawa, M. Umetsu, I. Kumagai, T. Adschiri, W. Hwang, W. Teizer, Biomed. Microdevices, 1–8 (2014a)

K. Kim, A. Sikora, K.S. Nakayama, H. Nakazawa, M. Umetsu, W. Hwang, W. Teizer, Appl. Phys. Lett. **105**, 143701 (2014b)

K. Kim, A. Sikora, K.S. Nakayama, M. Umetsu, W. Hwang, W. Teizer, J. Appl. Phys. **117**, 144701 (2015)

A. Maloney, L.J. Herskowitz, S.J. Koch, PLoS ONE **6**, e19522 (2011)

S.G. Moorjani, L. Jia, T.N. Jackson, W.O. Hancock, Nano Lett. **3**, 633–637 (2003)

J. Noel, W. Teizer, W. Hwang, ACS Nano **3**, 1938–1946 (2009)

D. Oliveira, D.M. Kim, M. Umetsu, I. Kumagai, T. Adschiri, W. Teizer, J. Appl. Phys. **112**, 124703 (2012)

J.B. Olmsted, G.G. Borisy, Biochemistry **14**, 2996–3005 (1975)

H.W.C. Postma, A. Sellmeijer, C. Dekker, Adv. Mater. **12**, 1299–1302 (2000)

L. Romberg, D.W. Pierce, R.D. Vale, J. Cell Biol. **140**, 1407–1416 (1998)

A. Sikora, D. Oliveira, K. Kim, A.L. Liao, M. Umetsu, I. Kumagai, T. Adschiri, W. Hwang, W. Teizer, Chem. Lett. **41**, 1215–1217 (2012)

A. Sikora, J. Ramón-Azcón, K. Kim, K. Reaves, H. Nakazawa, M. Umetsu, I. Kumagai, T. Adschiri, H. Shiku, T. Matsue, W. Hwang, W. Teizer, Nano Lett. **14**, 876–881 (2014)

K. Svoboda, S.M. Block, Cell **77**, 773–784 (1994)